Cryogenic 3D Printing of Heterogeneous Scaffolds with Gradient Mechanical Strengths and Spatial Delivery of Osteogenic Peptide/TGF-β1 for Osteochondral Tissue Regeneration

Chong Wang[1,†,*], Haibing Yue[2,†], Wei Huang[3,†], Xudong Lin[4,†], Xiaoqiong Xie[1], Zhi He[1], Xiao He[1], Sanbiao Liu[5], Lu Bai[5,*], Bingheng Lu[1], Yen Wei[1,6], Min Wang[7,*]

[1] College of Mechanical Engineering, Dongguan University of Technology, Dongguan, Guangdong, P.R. China

[2] Dr. Li Dak-Sum Research Centre, The University of Hong Kong-Karolinska Institutet Collaboration in Regenerative Medicine, The University of Hong Kong, 5 Sassoon Road, Hong Kong, HKSAR, P.R. China

[3] Department of Orthopedics, Union Hospital, Tongji Medical College, Huazhong University of Science and Technology, Wuhan, Hubei, P.R. China

[4] School of Biomedical Engineering, Sun Yat-Sen University, Guangzhou, Guangdong, P.R.China

[5] Department of Sports Medicine Shenzhen Hospital of Peking University, Shenzhen, Guangdong, P.R. China

[6] Department of Chemistry, Tsinghua University, Beijing, P.R. China

[7] Department of Mechanical Engineering, The University of Hong Kong, Pokfulam Road, Hong Kong, P.R. China

Keywords: *cryogenic 3D printing; osteogenic peptide; TGF-β1; osteochondral regeneration; osteogenic/chondrogenic differentiation*

*Corresponding authors, Dr. Wang Chong, School of Mechanical Engineering, Dongguan University of Technology, Email: wangchong@dgut.edu.cn; Dr. Bai Lu, Department of Sports Medicine Shenzhen Hospital of Peking University, Email: boowboow@163.com; Prof. Wang Min, The University of Hong Kong, Email: memwang@hku.hk. †Wang C, †Yue HB, †Huang W and †Lin X contributed equally.

Abstract

Due to the increasing aging population and the high probability of sport injury among young people nowadays, it is of great demand to repair/regenerate diseased/defected osteochondral tissue. Given that osteochondral tissue mainly consists of a subchondral layer and a cartilage layer which are structurally heterogeneous and mechanically distinct, developing a biomimetic bi-phasic scaffold with excellent bonding strength to regenerate osteochondral tissue is highly desirable. Three-dimensional (3D) printing is advantageous in producing scaffolds with customized shape, designed structure/composition gradients and hence can be used to produce heterogeneous scaffolds for osteochondral tissue regeneration. In this study, bi-layered osteochondral scaffolds were developed through cryogenic 3D printing, in which osteogenic peptide/β-tricalcium phosphate/poly(lactic-*co*-glycolic acid) water-in-oil composite emulsions were printed into hierarchically porous subchondral layer while poly(D,L-lactic acid-*co*-trimethylene carbonate) water-in-oil emulsions were printed into thermal-responsive cartilage frame on top of the subchondral layer. The cartilage frame was further filled/dispensed with transforming growth factor-β1 loaded collagen I hydrogel to form the cartilage module. Although the continuously constructed osteochondral scaffolds had distinct microscopic morphologies and varied mechanical properties at the subchondral zone and cartilage zone at 37 ^{o}C, respectively, the two layers were closely bonded together, showing excellent shear strength and peeling strength. Rat bone marrow derived mesenchymal stem cells (rBMSCs) exhibited high viability and proliferation at both subchondral- and cartilage layer. Moreover, gradient rBMSC osteogenic/chondrogenic differentiation was obtained in the osteochondral scaffolds. This proof-of-concept study provides a facile way to produce integrated osteochondral scaffolds for concurrently directing rBMSC osteogenic/chondrogenic differentiation at different regions.

Introduction

Degenerative osteoarthropathy and traumatic injury to osteochondral tissue have gained increasing attention nowadays[1,2]. Osteochondral tissue has a gradient structure, briefly consisting of a subchondral layer and a cartilage layer, which are closely bonded together[3]. As long-term injury of either subchondral layer or cartilage layer eventually results in the defects of the overall osteochondral tissue, appropriate strategy is urgently needed to reconstruct the integral osteochondral tissue[4]. Bone marrow stimulation has been used clinically to repair articular cartilage, however, limited repair efficiency with a low stability is often obtained. Among different treatments, scaffold-based tissue engineering has emerged as a leading strategy to regenerate osteochondral tissue[5-7]. Isotropic scaffolds and bi-phasic scaffolds consisting of simply sewed or piled subchondral layer and cartilage layer have been fabricated to repair osteochondral tissue. However, as the isotropic scaffold lacks of gradient of structure and heterogeneous mechanical strength and the bi-phasic scaffold lacks of strong interfacial bonding strength, successful application of isotropic- and bi-phasic scaffolds in osteochondral regeneration has been restricted[8-10].

Three-dimensional (3D) printing has emerged as a promising technique to fabricate tissue engineering scaffolds with desirable features such as customized shape, designed structure, suitable mechanical properties and even excellent biological activity[11-14]. However, features such as sufficient mechanical strength, biomimetic structure and controlled release of bioactive molecules, which are critical to induce favorable cellular responses, are relatively hard to be integrated into the same 3D printed scaffolds. For instance, scaffolds made through fused deposition modeling (FDM), selective laser sintering (SLS) and micro-extrusion of biomceramic pastes followed by sintering have relatively high mechanical strength, but they are lack of

biomimetic structure and incapable of loading high-dose induction molecules due to the high temperature involved in the printing process[15,16,17]. Hydrogels are capable of biomolecule/cell delivery, but the mechanical strength is insufficient for hard tissue repair[18,19]. Recently, cryogenic 3D printing, a new 3D printing technique has been increasingly used to produce tissue engineering scaffolds with superior features. Comparing to scaffolds made through other existing 3D printing techniques, cryogenic 3D printed scaffolds not only exhibit excellent mechanical strength to bear certain load but also have a biomimetic hierarchical porous structure to elicit improved cell responses[20,21]. Moreover, *in situ* delivery of bio-agents with a high loading level and a high biological activity can be achieved to induce improved cell differentiation[22]. By adjusting the polyester concentration and water content in the emulsions, the diameter of the micropores can be tuned. If bioceramic particles are involved in emulsions, scaffolds with better mechanical strength can be obtained for hard tissue repair[23].

Toward to construction of osteochondral tissue engineering scaffolds which have a much more complex structure, different strategies have been adopted. Shim *et al.* produced a multilayered poly(ε-caprolactone) (PCL) construct via FDM, followed by the addition of human bone marrow derived mesenchymal stem cells (hBMSCs)-laden hydrogel containing growth factors to induce osteochondral regeneration. The presence of PCL scaffolds acted as mechanical supports for cells and regenerated tissues while the osteogenic/chondrogenic differentiation of hBMSCs was tuned by the distribution of bone morphogenetic protein-2/transforming growth factor-β (BMP-2/TGF-β) as well as the hydroxyapatite in the hydrogel[24]. However, neither heterogeneous structures nor varied mechanical properties were designed in the osteochondral scaffolds. Given that the natural subchondral layer is mechanically and structurally similar to cancellous bone, a hierarchically porous scaffold with high compressive strength and *in situ* delivery of osteogenic

agents would be desirable to induce *in vitro* osteogenic differentiation of MSCs and *in vivo* subchondral bone regeneration[25]. On the other hand, as the natural cartilage layer of the osteochondral tissue is soft and elastic and contains no micropores under normal physiological condition, a variety types of hydrogels incorporated with bio-agents can be used to induce *in vitro* chondrogenic differentiation of MSCs and *in vivo* cartilage regeneration[26]. Besides, stable bonding between the subchondral layer and the hydrogel-like cartilage layer is required to guarantee the successful reconstruction of integrated osteochondral scaffolds.

Herein, we developed a bi-phasic osteochondral tissue engineering scaffold based on a composite design which combines closely bonded subchondral layer and cartilage layer. Osteogenic peptide/tricalcium phosphate/poly(D,L-lactic-*co*-glycolic acid) (peptide/TCP/PLGA) scaffolds which were hierarchically porous and mechanical similar to cancellous bone were produced via cryogenic 3D printing to create a osteogenic platform for rat BMSC (rBMSC) assembly and differentiation; thermal-responsive poly(D,L-lactic acid-*co*-trimethylene carbonate) (P(DLLA-TMC)) frame was printed on top of the subchondral layer to provide sufficient bonding strength between the cartilage layer and the subchondral layer; TGF-β1 containing collagen I hydrogel was dispensed in the macropores of shape memory P(DLLA-TMC) frame to create a local environment for rBMSC assembly and chondrogenic differentiation. We found that the osteochondral scaffolds had heterogeneous microstructures and gradient mechanical properties. Improved chondrogenic differentiation of rBMSCs at the cartilage layer was achieved by showing up-regulated expression of chondrogenic markers, chondrogenic gene expression and the production of glycosaminoglycan (GAG), while enhanced osteogenic differentiation of rBMSCs at the subchondral layer was obtained by showing up-regulated expression RUNX2, osteocalcin and alkaline phosphatase (ALP), related gene expression and calcium deposition.

Experimental

Materials

PLGA (LA: GA=50: 50, inherent viscosity of 0.76dL/g) and shape memory P(DLLA-TMC) (DLLA: TMC= 80:20, inherent viscosity of 0.76dL/g, transition temperature (T_{trans}): 37 ^{o}C) were provided by Jinan Daigang Biotechnology Ltd, Jinan, Shandong, China. β-tricalcium phosphate particles with an average diameter of 200 ± 20 nm were Aladdin Industrial Corporation products (Shanghai, China). Deionized (DI) water for all experiments was obtained using a DI water producer (Sartorius arium mini plus, Germany). Tween 20, phosphate buffered saline (PBS) tablets, bovine serum albumin (BSA) and TGF-β1 were Sigma-Aldrich products (USA). Dichloromethane (DCM) was supplied by Uni Chem Co., Korea. Collagen I (from rat tail) was Corning product (USA). Oesteogenic peptide (P24) with a sequence of KIPKA SSVPT ELSAI STLYL SGGC and a purity of 98.12% was synthesized by Shanghai Ziyu Biotechnology LTD, China.

Formation of inks to print subchondral layer and cartilage layer

Firstly, 2 mL of DI water was blended with 10 mL of PLGA/DCM solution (30%, w/v), 50 μL of Tween 20 and 3 g of TCP. After 5 min ultra-sonication, water-in-oil composite emulsion inks with uniform TCP distribution were successfully formed. 500 μL of DI water containing 5 mg of peptide and 5 mg of BSA (stabilizer) was then added into the TCP/PLGA/DCM emulsion, followed by 5 min of mixing, hence forming the inks for making subchondral layer. Secondly, 0.5 mL of DI water was blended with 5 mL of P(DLLA-TMC)/DCM solution (30%, w/v) and 10 μL of Tween 20. After 5 min ultra-sonication, uniform water-in-oil emulsion inks for printing the cartilage frame were formed. Thirdly, to fill the pores of the cartilage frame with hydrogels, 20 μg of TGF-β1 and 23 μL of NaOH (1 N) were added in 1 mL of collagen I solution (9 mg/mL) to

form neutralized TGF-β1/collagen I hydrogel precursor at 4 °C.

Cryogenic 3D printing of osteochondral scaffolds

Scaffolds with a cylindrical shape and a gradient structure were constructed in a cryogenic environment (i.e., -30 °C), according to a digital STL file. Typically, 8 layers of subchondral struts were printed first, followed by the continuous printing of 4 layers of cartilage frame struts. Each layer consisted of 10 paralleled rods with a length between 2 to 10 mm and a diameter of 0.4 mm; the distance between 2 paralleled rods was 0.4 mm; rods in adjacent layers had a cross angle of 90°. The struts in the top level of the subchondral scaffold were parallel to that in the bottom level of cartilage frame, thus enabling excellent bonding between the subchondral struts and the cartilage struts. After cryogenic 3D printing, the "frozen" scaffolds (still on the cryogenic platform) were cryo-dried in a fume hood for 1 h to remove DCM. After the production of osteochondral patterns, TGF-β1/collagen I hydrogel was dispensed into the macropores of the cartilage frame, followed by gelling treatment of the hydrogel at 37 °C for 30 min, hence forming integrated osteochondral scaffolds with both subchondral layer and cartilage layer. The osteochondral scaffolds were then freeze-dried for 24 h and stored at 4 °C.

Physical characterizations of scaffolds

The macroscopic morphology of scaffolds was examined using a digital camera (Huawei P20 Pro, China). The microstructure of scaffolds was observed using SEM (Leo 1530 Gemini, Zeiss, Oberkochen, Germany), in which scaffold samples were freeze-dried, followed by coating of a thin layer of gold. Osteochondral scaffolds as well as subchondral- and cartilage controls were subjected to compression testing under wet conditions at 37 °C. 5 samples with a dimension of 10 mm ×10 mm ×10 mm were tested for each type of scaffold and the strain speed was set as 1 mm/min. The bonding strength between subchondral layer and cartilage layer was examined by

shear testing and peel testing. Towards shear testing, lap shear ASTM D3163 testing is followed. The overlap length was 12.7 mm and the strain speed was set as 1.3 mm/min. Towards the peel testing, ASTM D3330 Method A (180 º peel) was followed.

***In vitro* release behavior of peptide and TGF-β1**

To investigate *in vitro* release of osteogenic peptide and TGF-β1, pre-weighed scaffold samples were put into test tubes filled with PBS solutions supplemented with additives (0.02% sodium azide, 0.1% BSA, 0.05% EDTA and 0.1% heparin). The test tubes were put in a shaking water bath at 37 ºC. At pre-determined time intervals, the test liquids were taken out. The concentration of TGF-β1 was measured using TGF-β1 ELISA Kit assay (Peprotech Inc., USA). To measure the release rate of osteogenic peptide, osteogenic peptide conjugated with FITC (osteogenic peptide-FITC) was used to form peptide containing scaffolds and the release rate of peptide-FITC was measured by examining the peptide-FITC concentration using a fluorescence microplate reader.

***In vitro* degradation behaviour of scaffolds**

In vitro scaffold degradation was investigated by monitoring the scaffold remaining weight (%) within an 8 week test period. Pre-weighed samples were immersed in PBS (pH 7.4) with 0.05 wt% sodium azide in tubes. The tubes were sealed and placed in a shaking water bath, which was maintained at 37 ºC and shaken horizontally at 30 rpm. At each time point (2, 4, 6, and 8 weeks), a group of test samples were taken out from the tubes and rinsed in DI water five times to remove salts, followed by a 48 h drying. The ratio between the remaining weight and initial weight of each sample was calculated, showing the percentage of the remaining weight.

Cell culture

rBMSCs were cultured with Dulbecco's modified Eagle's medium/F-12, (DMEM/F-12, Gibco,

USA) which was supplemented with 10% fetal bovine serum (Gibco, USA), 100 U/ml penicillin-streptomycin and 2 mM L-glutamine (Invitrogen, USA) and maintained in a humidified incubator at 37 ^{o}C with 5% CO_2. The medium was changed every 2 days. After the fabrication of the osteochondral scaffolds, 0.2 mL of rBMSCs solution with a concentration $1*10^6$ cell/mL was dispensed on both sides of the freeze-dried osteochondral tissue constructs to allow rBMSC seeding into the subchondral and cartilage zones.

Cell viability and proliferation

A live and dead viability kit (Molecular Probes, USA) was used to stain cells to investigate the cyto-compatibility of osteochondral scaffolds. For cell staining, cell-scaffold constructs were washed and incubated in DMEM/F-12 containing 4 μM EthD-1 and 2 μM calcein AM in a humidified incubator (37 °C, 5% CO_2) for 15 min, where live cells and dead cells were stained into green color and red color, respectively. Fluorescence images of cell-scaffold constructs were obtained using a fluorescence microscope (Nikon Eclipse TE2000-U inverted microscope, Japan) The cell survival rate at each time point (1 and 3 days) was calculated. The proliferation of rBMSCs in both cartilage layer and subchondral layer was examined using CCK8 assay after 1, 4 and 7 days of culture.

Immunofluorescence staining of chondrogenic and osteogenic markers

After 14-day culture, rBMSC-laden osteochondral scaffolds were subjected to staining of nucleus, F-actin and chondrogenic markers including sry related HMG box protein-9 (SOX9), collagen II (COL II) and aggrecan (ACAN), whereas the the expression of osteogenic markers including Runt-related transcription factor 2 (RUNX2) and osteocalcin (OCN) in rBMSC-laden osteochondral scaffolds were also labeled via immuofluorescence staining. Cell-scaffold constructs were first fixed with 4% polyformaldehyde (PFA). After washing with PBS, the cells

were permeabilized in 0.2% Triton X-100 solution and incubated in (1% w/v) BSA block solution, followed by the incubation in SOX9,COL II, ACAN, RUNX2 or OCN monoclonal antibody (Boster Biological Technology co., Ltd, China) containing block solution (BSA solution (1%, w/v), Sigma-Aldrich, USA) for 1 h. After washing with PBS, rBMSC-laden scaffolds were incubated in aqueous solution of Alexa Fluor(r) 555 Goat Anti-Rabbit IgG (H+L) (Life technologies, USA) for 1 h. Alexa Fluor 488 phalloidin (Molecular Probes, USA) was simultaneously added to the solution for the F-actin staining. With another washing, samples were added with 4',6-diamidino-2-phenylindole (DAPI, Life Technologies) solutions and subjected to a confocal laser scanning microscope (CLSM, LSM 710 Meta, Carl Zeiss, Germany) for observations of nucleus, F-actin filaments and chondrogenic/osteogenic markers. The expression of chondrogenic/osteogenic markers on both the subchondral layer and the cartilage layer was observed.

Histochemical staining

To investigate the osteogenic differentiation of rBMSCs, the extracts of subchondral layer scaffolds and cartilage layer scaffolds were used to culture rBMSCs for 14 days in tissue culture plates, respectively. At the predetermined time points, cells were fixed with 4% PFA for 4 h and alkaline phosphatase (ALP) staining was performed by using the ALP leukocyte kit (Sigma, USA). The stained cells were observed under an inverted microscope (Nikon Eclipse TE2000-U, Japan). Similarly, after 21-day culture, 2% Alizarin Red S (ARS) working solution (pH 4.1-4.3) was added for the 30 min staining at room temperature to stain the deposited calcium minerals. With further washes, the stained cells were observed under an inverted microscope (Nikon Eclipse TE2000-U, Japan). Towards the production of glycosaminoglycan (GAG), after 2 weeks of culture, toluidine blue and sarfranin O (Boster, China) were used to stain the fixed cell-laden

osteochondral tissue engineering scaffolds to visualize the GAG in the osteochondral scaffolds.

Osteogenic/chondrogenic gene expression of rBMSCs

rBMSCs were seeded on scaffolds for 14 days and Trizol (Thermofisher Scientific, USA) was used to extract mRNA from the cells. The reverse transcription procedure was carried out by TaqMan MicroRNA Reverse Transcription Kit (Thermofisher Scientific, USA). Quantitative polymerase chain reaction (qPCR) Sybn Green Master Mix (Thermofisher Scientific, USA), forward and reverse primers and cDNA were loaded onto a 96-well plate, and the real time-PCR (RT-PCR) procedure was performed in ABI 7900HT Sequence Detection System. The primer sequence is shown in Table 1. The qPCR data was analyzed using $2^{-\Delta\Delta Ct}$ method.

Table 1 Primers used in qPCR analysis

Gene	Sequence
GAPDH: (F)	5’-ACCACAGTCCATGCCATCAC-3’
GAPDH: (R)	5’-TCCACCACCCTGTTGCTGTA-3’
ALP: (F)	5’-GTCCCACAAGAGCCCACAAT-3’
ALP: (R)	5’-CAACGGCAGAGCCAGGAAT-3’
OSTEOCALCIN: (F)	5’-GGGCAATAAGGTAGTGAA-3’
OSTEOCALCIN: (R)	5’-GTAGATGCGTTTGTAGGC-3’
RUNX2: (F)	5’-CCACCTCTGACTTCTGCCTC-3’
RUNX2: (R)	5’-TATGGAGTGCTGCTGGTCTG-3’
SOX9: (F)	5’-CACAAGAAAGACCACCCCGA-3’
SOX9: (R)	5’-TGCACGTCTGTTTTGGGAGT-3’
COL II: (F)	5’-GGCCAGGATGCCCGAAAATTAG-3’
COL II: (R)	5’-ACCCCTCTCTCCCTTGTCAC-3’
AGGRECAN: (F)	5’-TACGACGCCATCTGCTACAC-3’
AGGRECAN: (R)	5’-TCGAAGATGGGCTTTGCAGT-3’

Statistical analysis

All statistical analyses were performed using the SPSS software (version18). Numerical data are presented as the mean value ± standard deviation (S.D.). For the statistical comparisons, one-way analysis of variance (ANOVA) with the Student’s t test was applied. p <0.05(*) was considered

to be statistically significant.

3. Results

3.1 Design of integrated osteochondral tissue engineering scaffolds

In the current study, an integrated osteochondral tissue engineering scaffold consisting of a subchondral layer and a cartilage layer was designed to regenerate osteochondral tissue. The illustrative schematic of making integrated osteochondral scaffolds is shown in **Fig.1**. Through cryogenic 3D printing of osteogenic peptide/TCP/PLGA/DCM inks (i.e., to form subchondral layer) and P(DLLA-TMC)/DCM inks (i.e., to form the cartilage frame), closely bonded subchondral layer and cartilage frame were produced. With further dispensing of TGF-β1/collagen I hydrogel into the cartilage frame, integrated osteochondral tissue engineering scaffolds which were structurally and mechanically similar to native osteochondral tissue can be obtained. The delivery of osteogenic peptide and TGF-β1 in the subchondral layer and cartilage layer, respectively, could spatially direct the osteogenic/chodrogenic differentiation of rBMSCs *in vitro*, hence enabling customized osteochondral tissue regeneration.

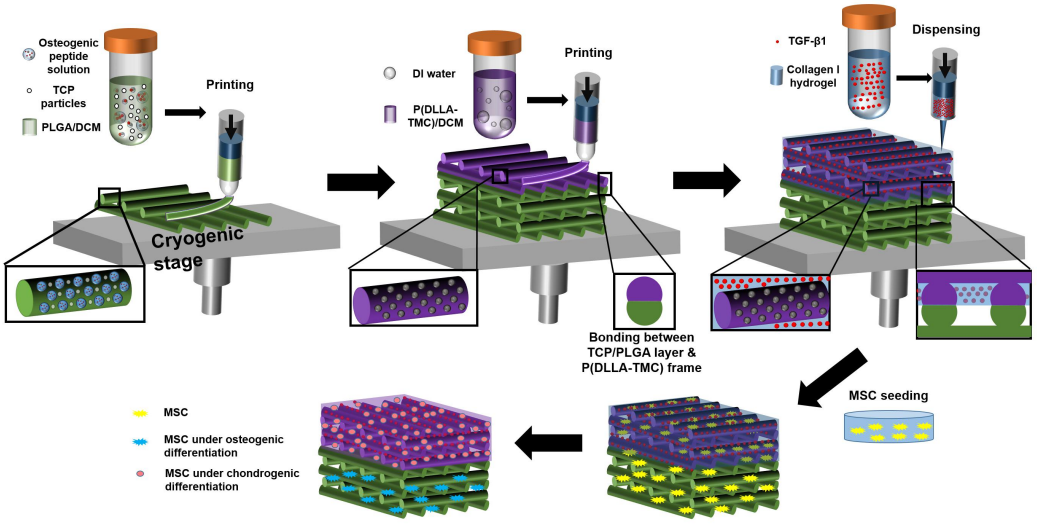

Fig.1 Illustrative schematic shows the fabrication process of integrated osteochondral tissue engineering scaffolds and seeding and osteogenic/chondrogenic differentiation of MSCs.

Fig.2a and **b** show the macro- and micromorphology of integrated osteochondral scaffolds as well as subchondral- and cartilage controls. The subchondral scaffold had a latticed structure and each strut had a microporous morphology, in which β-TCP particles were uniformly distributed on the strut surface. P(DLLA-TMC) frame, a key component of the cartilage layer, was printed over the as-printed subchondral layer. The P(DLLA-TMC) frame also had a latticed structure, but the strut diameter was smaller than that in subchondral layer. Numerous micropores were observed on surface of the P(DLLA-TMC) frame. Uniform and exclusive distribution of elements such as Ca and P was observed in the subchondral layer but not in the P(DLLA-TMC) frame in the cartilage layer (**Fig.2c**). After 3D printing of the cartilage frame, TGF-β1 containing collagen I hydrogel (color in pink) was dispensed into the macropores of P(DLLA-TMC) frame, showing a typical hydrogel morphology.

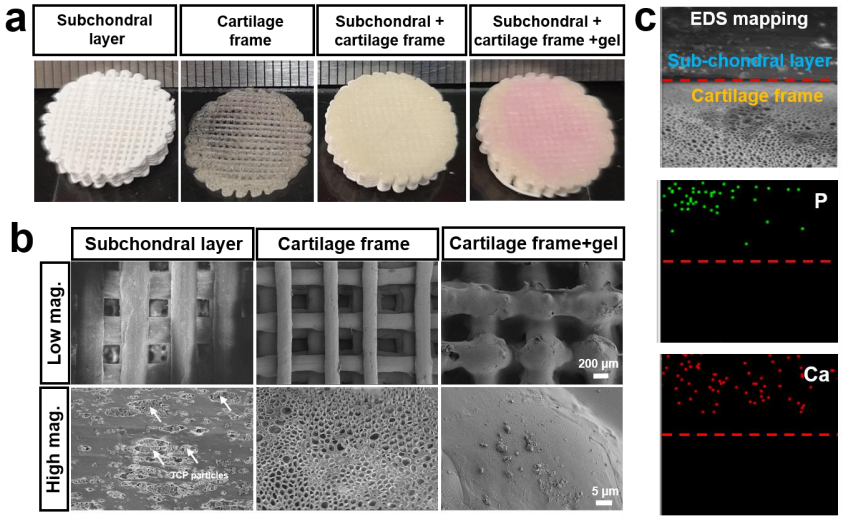

Fig.2 Morphology of integrated osteochondral tissue engineering scaffolds. (a) digital graphs of osteochondral scaffolds and controls; (b) SEM micrographs of different layers of osteochondral scaffolds; (c) EDS elemental mapping of Ca and P at the subchondral layer/cartilage frame interface.

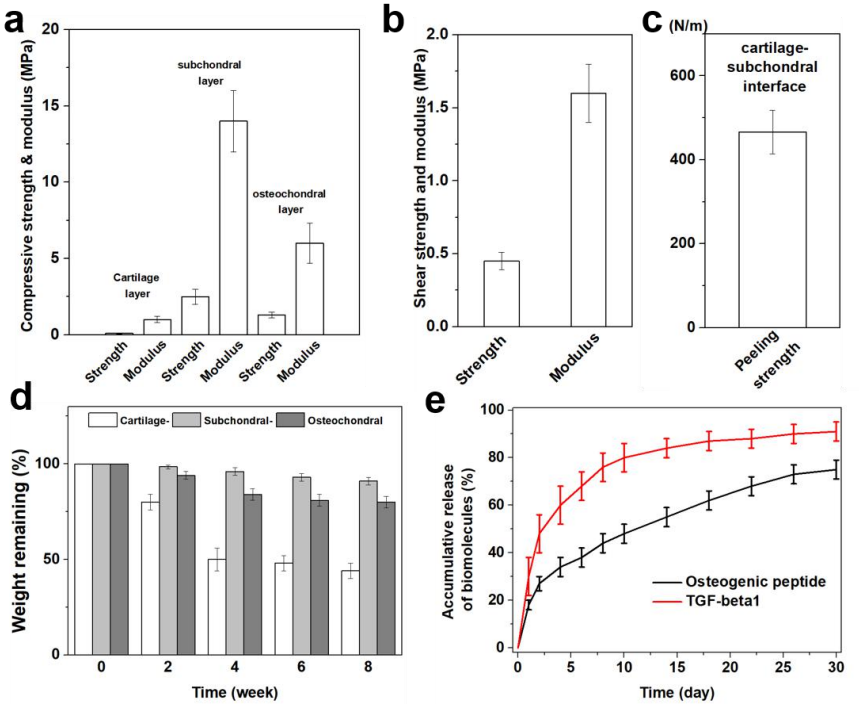

Fig.3 Mechanical properties, *in vitro* degradation behaviour and *in vitro* release behaviour of osteochondral scaffolds. (a) compressive strength and modulus of osteochondral scaffolds and controls under wet condition at 37 ºC; (b) shear strength and modulus of osteochondral interface under wet condition at 37 ºC; (c) peel strength of osteochondral interface under wet condition at 37 ºC; (d) *in vitro* degradation of scaffolds; (e) *in vitro* release of peptide and TGF-β1.

The compressive strength and elastic modulus of osteochondral tissue engineering scaffolds were investigated under wet condition at 37 ºC. The subchondral layer had a mechanical strength of 2.4 MPa and an elastic modulus of 14.1 MPa, which were comparable to that of human cancellous bone (strength: 4-12 MPa; elastic modulus: 50-500 MPa) (**Fig.3a**)[27]. In comparison, the whole cartilage layer (i.e., consisting of P(DLLA-TMC) frame and collagen I hydrogel) had a compressive strength and an elastic modulus of 0.12 MPa and 1.05 MPa, respectively, which were significantly lower than that of the subchondral layer ($p < 0.05$), but similar to that of the human cartilage tissue (compressive modulus: 0.4-1.0 MPa)[28]. The compressive strength and

modulus of the integrated osteochondral tissue engineering scaffolds were lower than that of subchondral control, but still significantly higher than that of the cartilage control ($p < 0.05$). The bonding strength between the subchondral layer and the cartilage layer was measured through shear testing and peeling testing along with the axial direction of the bonded subchondral struts and cartilage struts (**Fig.S1**). The shear strength between cartilage layer and the subchondral layer was 0.4 MPa at 37 ^{o}C, showing a shear modulus of 1.6 MPa (**Fig.3b**). The osteochondral interface also showed a peel strength of 470 N/m at 37 ^{o}C (**Fig.3c**), suggesting that cryogenic 3D printing is a superior technique to produce bi-phasic osteochondral scaffolds with sufficient interfacial bonding strength. *In vitro* degradation behaviour of osteochondral scaffolds was subsequently investigated by monitoring the scaffold weight remaining within an 8-week test period. The subchondral layer alone showed a weight loss of 2, 5 and 12% after 2, 4 and 8 week incubation, respectively. The continuously increased weight loss could be attributed to the hydrolysis of PLGA matrices and the decomposition of embedded β-TCP (**Fig.3d**). The cartilage layer showed much higher weight loss percentage (> 50%) within 8 weeks, and this could be mainly attributed the degradation of collagen I hydrogel and slow hydrolysis of P(DLLA-TMC). In comparison, the osteochondral scaffolds exhibited a moderate level of *in vitro* degradation. The *In vitro* release behaviour of osteogenic peptide and TGF-β1 from the subchondral zone and the cartilage module was investigated in a 30-day period (**Fig.3e**). Peptide was released from the subchondral scaffolds in a sustained manner, in which initial burst release up to 25% was observed in 48 h, followed by a slower but steady release up to 70% within 30 days. In comparison, TGF-β1 showed a quicker release by showing 47% initial release within 48 h, followed by a slower but sustained release up to 90% within 30 days.

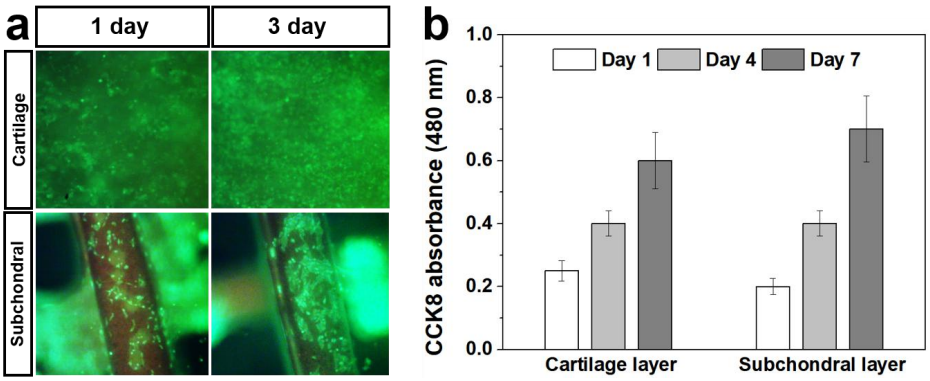

Fig.4 Viability of rBMSCs in osteochondral scaffolds *in vitro*. (a) live and dead staining of rBMSCs in cartilage layer and subchondral layer of the integrated osteochondral tissue engineering scaffolds; (b) CCK8 absorbance of rBMSCs cultured in cartilage layer and subchondral layer of integrated osteochondral tissue engineering scaffolds.

The biological performance of integrated osteochondral tissue engineering scaffolds was first evaluated by studying the viability of rBMSCs located at different regions. After 1 or 3-day culture, most rBMSCs (color in green) with an expanded shape were found in the subchondral layer and only a few dead cells (color in red) could be observed, suggesting that subchondral scaffolds were cytocompatible (**Fig.4a**). Likewise, most rBMSCs in the collagen I hydrogel were also alive (color in green), showing a rounded shape, indicating that the cartilage layer was also a desirable environment for rBMSC survival. Meanwhile, increased CCK8 absorbance was obtained for rBMSCs cultured both at the subchondral layer and the cartilage layer with increasing culture time, suggesting that the osteochondral tissue scaffold was a favorable platform for rBMSC proliferation (**Fig.4b**).

Whether osteogenic or chondrogenic differentiation of rBMSCs at respective region of the integrated osteochondral scaffolds could be effectively and simultaneously induced is of great importance. On one hand, the chondrogenic differentiation of rBMSCs at the cartilage layer and the subchondral layer of the integrated osteochondral tissue engineering scaffolds was

investigated by visualizing the expression of SOX9, COL II and ACAN through immunuofluorescence staining, followed by confocal laser scanning microscopy (CLSM) observations. After 14 days of culture, significantly up-regulated expression of SOX9, COL II and ACAN was observed in the cartilage zone of integrated osteochondral scaffolds incorporated with TGF-β1 (**Fig.5a**), whereas less expression of SOX9, COL II and ACAN were observed in the cartilage zone without TGF-β1. In comparison, no SOX9 expression and very limited expression of collagen II and ACAN were observed in the subchondral zone, suggesting that the combination of enclosed soft environment (i.e., collagen I hydrogel) with the controlled delivery of chondrogenic agents had an synergistic effect on the chondrogenic differentiation of rBMSCs. On the contrary, porous bony environment with higher modulus with the presence of osteogenic molecules had little supportive effect on rBMSC chondrogenic differentiation. This was further confirmed by the gene expression of SOX9, COL II and ACAN after 14 days of culture, in which cartilage zone containing TGF-β1 induced the highest expression level of chondrogenic genes (**Fig.5b** to **d**), whereas the subchondral zone induced very limited expression of SOX9, ACAN and COL II genes.

Towards the rBMSC osteogenic differentiation, the expression of runt-related transcription factor 2 (RUNX2) and osteocalcin (OCN) was studied via immunofluorescence staining after 14 days of culture (**Fig.6c**). Obvious expression of RUNX2 and OCN was observed in subchondral zone containing peptide, whereas lowered expression level of RUNX2 and OCN was found in subchondral zone without peptide incorporation. In comparison, limited expression of RUNX2 and OCN was observed in cartilage zone with or without TGF-β1 encapsulation. ALP staining and Alizarin Red S (ARS) staining were also conducted to study the osteogenic differentiation of rBMSCs as well as the cell mineralization. Compared to the extracts of the cartilage module, the

extracts of subchondral layer significantly up-regulated ALP expression of rBMSCs after 14 days (color in violet) and subchondral zone containing peptide induced the highest level of ALP expression (**Fig.6c**). After 21 days of culture, the exacts of subchondral layer containing peptide induced higher amount of calcium deposition than that of the cartilage module (**Fig.6d**). The gene expression of RUNX2, ALP and OCN showed the same trend, in which the subchondral zone containing peptide had the highest expression level, whereas significantly lowered osteogenic gene expression was observed in cartilage zone with or without TGF-β1 incorporation (**Fig.6e** to **g**).

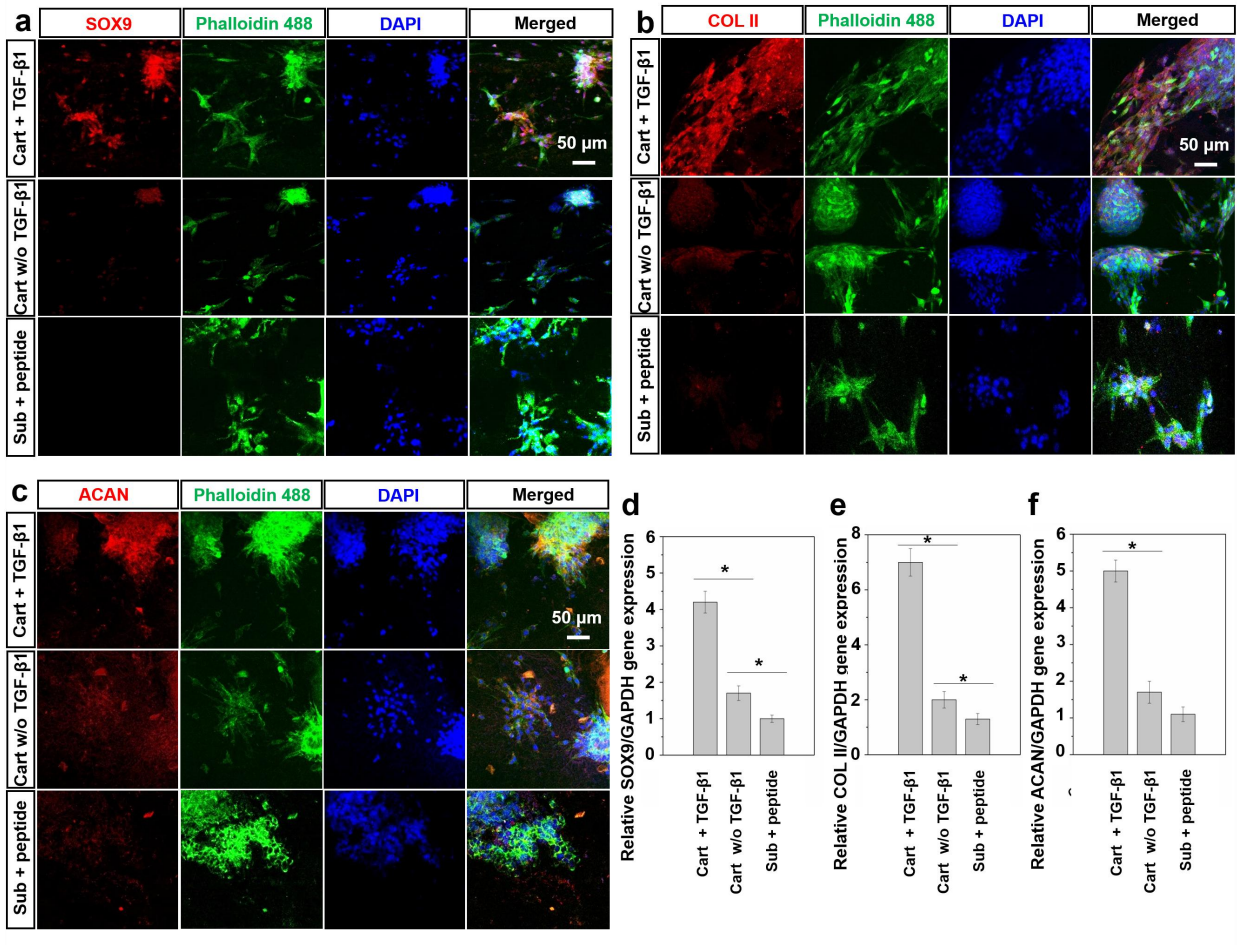

Fig.5 Immunofluorescence staining of chondrogenic markers in rBMSCs in integrated osteochondral tissue engineering scaffolds after 14 days of culture. (a-c) expression of

chondrogenic markers including sry related HMG box protein-9 (SOX9), collagen II (COL II) and aggrecan (ACAN) at different regions of integrated osteochondral tissue engineering scaffolds; (d-f) expression of chondrogenic genes including SOX9, COL II and ACAN in rBMSCs located at different regions of integrated osteochondral tissue engineering scaffolds.

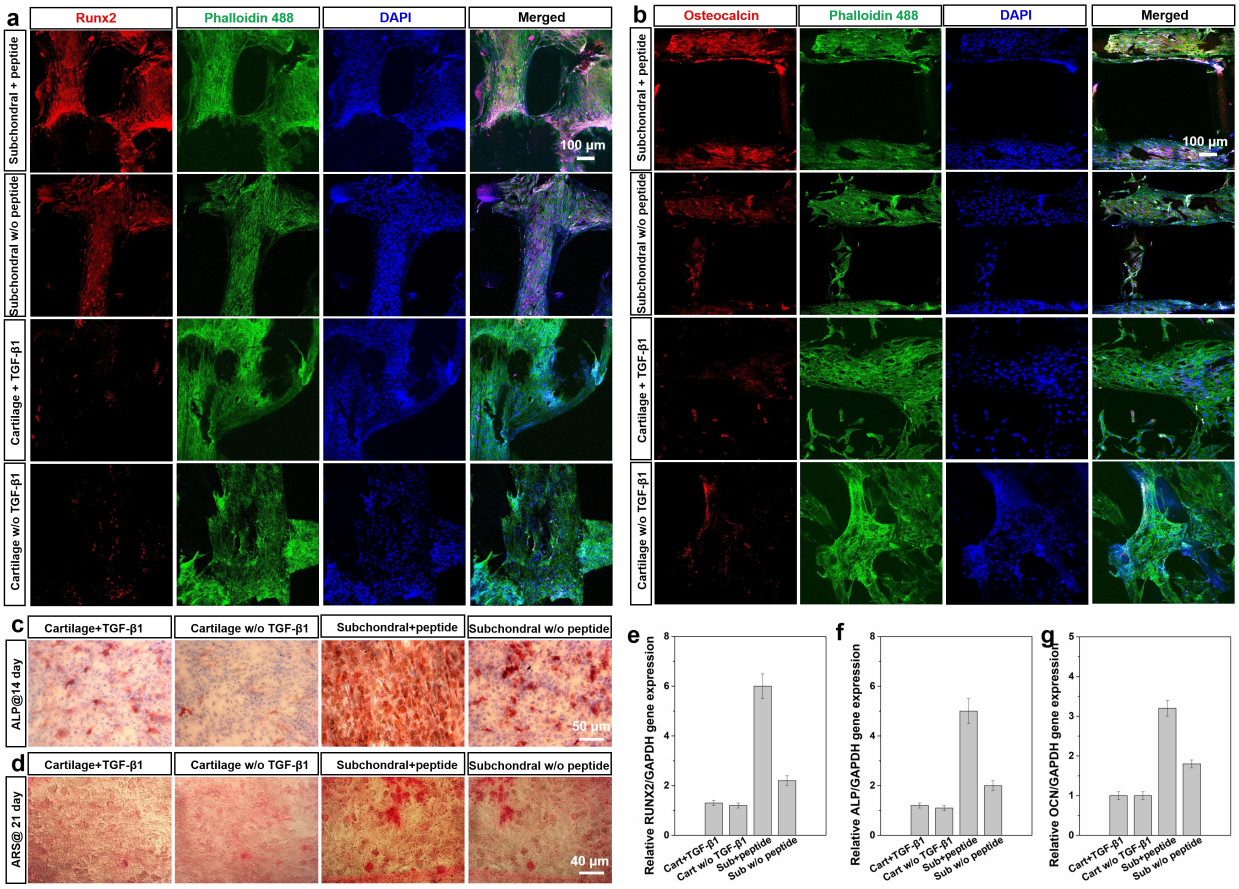

Fig.6 Osteogenic differentiation of rBMSCs in cartilage layer and subchondral layer of integrated osteochondral tissue engineering scaffolds: (a) immunofluorescence staining of RUNX2 in rBMSCs in osteochondral tissue engineering scaffolds after 14 days of culture; (b) immunofluorescence staining of osteocalcin (OCN) in rBMSCs in osteochondral tissue engineering scaffolds after 14 days of culture; (c) ALP staining of rBMSCs cultured in extracts of cartilage zone or subchondral zone for 14 days; (d) ARS staining of rBMSCs cultured in extracts of cartilage zone or subchondral zone for 21 days; (e-g) expression of osteogenic genes

including RUNX2, ALP and OCN in rBMSCs located at different regions of integrated osteochondral scaffolds.

After 14 days of culture, the production of GAG at the cartilage layer of the osteochondral scaffolds was visualized via staining of sarfranin O and toluidine blue. Pink color and dark blue color were observed in cartilage layer of the osteochondral scaffolds with TGF-β1 incorporation (**Fig.7**). In comparison, when no TGF-β1 were loaded, much lighter pink and blue colors can be observed. These results indicate that the hydrogel-like microenvironment could slightly support GAG production while the controlled delivery of TGF-β1 could significantly improve GAG production. The cartilage controls showed the same trend, suggesting that the integration of cartilage layer and subchondral layer to form an osteochondral scaffold would not affect the GAG production at the cartilage zone.

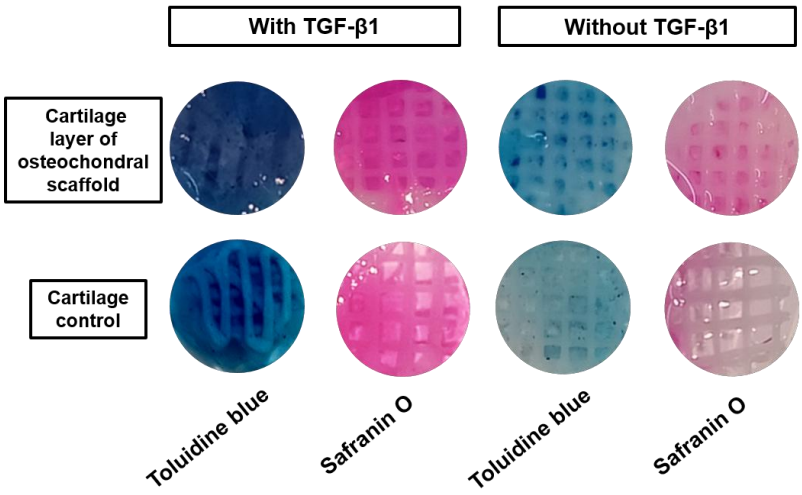

Fig.7 Staining of sarfranin O and toluidine blue to visualize the formation of glycosaminoglycan (GAG) at the cartilage layer of the osteochondral scaffolds with or without TGF-β1 incorporation after 14 days of culture.

Discussion

In natural osteochondral tissue, the composition, structure and mechanical properties of closely

bonded subchondral layer and cartilage layer are distinct. Therefore, to better mimic the heterogeneous features of the natural osteochondral tissue and hence to improve the osteochondral tissue regeneration, an engineered osteochondral scaffold consisting of closely bonded subchondral layer and cartilage layer, which could mimic the natural subchondral tissue and cartilage tissue, respectively, is strongly needed[29-33]. Given that the opening level of cellular environment and the matrix stiffness could affect the cell morphogenesis and hence influence the differentiation direction of MSCs, the integration of a hierarchically porous and high-strength subchondral layer with an elastic hydrogel-like cartilage layer could direct MSC morphogenesis along osteogenic lineage and chondrogenic lineage spatially. Moreover, the controlled deliver of osteogenic/chondrogenic growth factors could significantly improve the spatial osteogenic/chondrogenic differentiation at respective region[34,35]. In this study, a bi-phasic scaffold consisting of peptide/TCP/PLGA subchondral layer and P(DLLA-TMC) cartilage frame could be produced through cryogenic 3D printing. With further dispensing of TGF-β1/collagen I hydrogel into the cartilage frame, integrated osteochondral scaffolds with the capability to spatially direct MSC osteogenic/chondrogenic differentiation could be obtained. Different from the scaffolds made through FDM, SLS and extrusion-based 3D printing followed by post-sintering, the subchondral scaffolds produced through cryogenic 3D printing were not only mechanically similar to human cancellous bone but also hierarchically porous and capable of *in situ* osteogenic peptide delivery[36,37]. Likewise, different from other cartilage layers solely made of hydrogel or synthetic polymers, our cartilage layer was comprising of both thermo-responsive shape memory P(DLLA-TMC) frame and TGF-β1-loaded collagen I hydrogel. The hydrogel acted as a biomimetic cellular environment for rBMSC assembly and subsequent chondrogenesis, whereas the P(DLLA-TMC) frame acted as a medium to enable tight bonding between the

subchondral layer and the cartilage layer. The presence of micropores on the surface of cartilage frame (i.e., P(DLLA-TMC) frame) could be attributed to both the formation of ice particles in the frozen struts and the solvent evaporation (i.e., DCM) induced phase separation. In our study, water-in-oil emulsions comprising of DI water droplets with a diameter of 5-10 microns and P(DLLA-TMC)/DCM with a certain concentration were formulated through ultra-sonication. The presence of water droplets in emulsions allows rapid freezing of the printing inks under a cryogenic environment, hence enabling the continuous layer-by-layer printing. Once the printing is completed, as-farbicated scaffolds are freeze-dried to remove DCM and water droplets, leaving numerous micropores on strut surface. In comparison, as a large number of TCP particles were blended with DI water/PLGA/DCM emulsions, much fewer micropores with a less regular shape can be found on the subchondral struts. As both PLGA and P(DLLA-TMC) were dissolved in DCM to formulate inks for the continuous 3D printing of the subchondral layer and the cartilage frame, the interfacial bonding strength between P(DLLA-TMC) and TCP/PLGA struts was greatly increased once the DCM was evaporated. Moreover, as P(DLLA-TMC) matrix was thermo-responsive, the P(DLLA-TMC) frame became soft at 37 ^{o}C, hence the engineered cartilage layer consisting of P(DLLA-TMC) frame and hydrogel was mechanically comparable to the native cartilage tissue[38,39]. Towards the scaffold degradation, as P(DLLA-TMC) frame had similar degradation rate to TCP/PLGA, the relatively fast degradation of the cartilage layer could be mainly attributed to two reasons: (1) the degradation of collagen I hydrogel blocks was faster than TCP/PLGA composite during long-term incubation; (2) no rBMSCs were seeded on the cartilage layer when the degradation experiments were conducted, hence no newly produced extracellular matrix and polysaccharide can be deposited on the cartilage layer to compensate the weight loss of the collagen I hydrogel. If rBMSCs were seeded on cartilage layer and cultured

for a relatively long period, slower degradation of the cartilage layer can be obtained. In future, hydrogels with slower degradation rate can be used to fabricate cartilage layer, in order to provide the cartilage layer with longer structural stability.

In addition to mimicking the natural osteochondral tissue from structural and mechanical aspects, providing osteochondral scaffolds with desirable biological performance is also of great importance. The initial peptide release from the subchondral layer could be attributed to the dissolution of peptide located on the surface of the struts at the outer area, while the sustained peptide release could be attributed to the diffusion of peptide released from the inner part of the subchondral scaffolds. In comparison, the faster TGF-β1 release could be attributed to the diffusion of TGF-β1 from the hydrogel to the subchondral region. To reduce the sudden release of TGF-β1, TGF-β1 could be incorporated in DI water/P(DLLA-TMC)/DCM emulsion inks to form TGF-β1 loaded P(DLLA-TMC) cartilage frame. The collagen I hydrogel would then act as a barrier to slow down the TGF-β1 release into the test liquid. Apart from providing excellent biocompatibility, whether the rBMSCs located at subchondral zone and cartilage zone can differentiate along with osteogenic- and chondrogenic lineages, respectively, is highly concerned[40,41]. The results showed that both the microstructure and the locally incorporated biologically active agents could affect the osteogenic/chondrogenic differentiation of rBMSCs. On one hand, as TCP and peptide were delivered in the hierarchically porous subchondral layer, the microporous bony environment with balanced osteoconductivity-osteoinductivity enhanced the osteogenic differentiation of local rBMSCs by showing up-regulated expression of RUNX2, ALP, and OCN, as well as the related genes**.** On the other hand, the presence of TGF-β1 in the enclosed hydrogel microenvironment enhanced the chondrogenic differentiation of rBMSCs by showing significantly up-regulated expression of SOX9, COL II and ACAN, as well as the

related genes[42,43]. This trend was further verified by the GAG production in osteochondral scaffolds, in which significantly higher amount of GAG was observed in the cartilage layer of TGF-β1 loaded osteochondral scaffolds than that without TGF-β1 incorporation, suggesting sustained TGF-β1 is crucial in directing chondrogenic differentiation of rBMSCs. Although rBMSCs located at the subchondral layer also had a very limited level of expression of COL II and ACAN, which could be attributed to the slight diffusion of TGF-β1 from cartilage layer to the culture medium, rBMSCs located at the subchondral layer primarily followed the osteogenic differentiation path. To reduce the cross effect of TGF-β1 on the osteogenic differentiation of rBMSCs in the subchondral layer, TGF-β1 should be restricted to cartilage layer alone, and this could be realized by incorporating TGF-β1 in hierarchically porous P(DLLA-TMC) frame. The diffusion of TGF-β1 released from the micropores into the culture medium could be then delayed by the hydrogel. Moreover, a calcified transition interface with a dense structure can be inserted between the chondral layer and the subchondral part to minimize the mutual diffusion of osteogenic peptide andTGF-β1 into the opposite region. This proof-of-concept study provides an facile way to produce biomimetic osteochondral scaffolds to concurrently direct the osteogenic and chondrogenic differentiation of MSCs at appropriate regions.

Conclusions

Biomimetic osteochondral scaffolds comprising of tightly bonded subchondral layer and cartilage layer were successfully produced through cryogenic 3D printing. The subchondral layer had a hierarchically porous structure and were mechanically similar to the native subchondral bone tissue whereas the P(DLLA-TMC)/collagen I composites could mimic the structure and mechanical properties of native cartilage tissue. The osteogenic differentiation of rBMSCs at the subchondral layer was improved due to the presence of TCP and peptide in the hierarchically

porous bony environment, whereas the chondrogenic differentiation of rBMSCs at the cartilage layer was improved due to enclosed hydrogel environment and the presence of TGF-β1, hence forming an engineered osteochondral tissue with heterogeneous structure, tuned mechanical properties and improved bone/cartilage forming ability. This proof-of-concept study further widens the way to produce tissue engineering scaffolds with heterogeneous features.

Acknowledgments

This work was supported by Dongguan University of Technology High-level Talents (Innovation Team) Research Project (KCYCXPT201603) and Dongguan University of Technology Research Team (TDYB2019003), Youth Innovative Talent Project from the Department of Education of Guangdong Province, China (2016KQNCX168), Natural Science Foundation of Guangdong Province, China (2018A0303130019).

References

[1] Krych AJ, Pareek A, King AH, Johnson NR, Stuart MJ, Williams RJ, Return to sport after the surgical management of articular cartilage lesions in the knee: a meta-analysis, Knee Surgery Sports Traumatology Arthroscopy,2017, 25(10), 3186-3196.

[2] van Haaften EE, Ito K, van Donkelaar CC, The Initial Repair Response of Articular Cartilage After Mechanically Induced Damage, Journal of Orthopaedic Research, 2017, 35(6), 1265-1273.

[3] Goldring SR, Goldring MB, Changes in the osteochondral unit during osteoarthritis: structure, function and cartilage-bone crosstal, Nature Reviews Rheumatology, 2016, 12(11), 632-644.

[4] Richter DL, Schenck RC, Wascher DC, Treme G, Knee Articular Cartilage Repair and Restoration Techniques: A Review of the Literature,Sports Health-A Multidisciplinary Approach, 2016, 8(2), 153-160.

[5] Liao JF, Tian TR, Shi SR, Xie XP, Ma QQ, Li G, Lin YF, The fabrication of biomimetic

biphasic CAN-PAC hydrogel with a seamless interfacial layer applied in osteochondral defect repair, Bone Resreach, 2017, 5, 17018.

[6] Makris EA, Gomoll AH, Malizos KN, Hu JC, Athanasiou KA, Repair and tissue engineering techniques for articular cartilage, Nature Reviews Rheumatology, 2015 11(1), 21-34.

[7] Yan LP, Silva-Correia J, Oliveira MB, Vilela C, Pereira H, Sousa RA, Mano JF, Oliveira AL, Oliveira JM, Reis RL, Bilayered silk/silk-nanoCaP scaffolds for osteochondral tissue engineering: In vitro and in vivo assessment of biological performance, Acta Biomaterialia, 2015,12, 227-241.

[8] Yousefi AM, Hoque ME, Prasad RGSV, Uth N, Current strategies in multiphasic scaffold design for osteochondral tissue engineering: A review. Journal of Biomedical Materials Research Part A, 2015, 103(7), 2460-2481.

[9] Marionneaux A, Walters J, Guo H, Mercuri J, Tailoring the subchondral bone phase of a multi-layered osteochondral construct to support bone healing and a cartilage analog, Acta Biomaterialia, 2018, 78, 351-364.

[10] Clearfield D, Nguyen A, Wei M, Biomimetic multidirectional scaffolds for zonal osteochondral tissue engineering via a lyophilization bonding approach, Journal of Biomedical Materials Research Part A, 2018, 106(4), 948-958.

[11] Kelly CN, Miller AT, Hollister SJ, Guldberg RE, Gall K, Design and Structure-Function Characterization of 3D Printed Synthetic Porous Biomaterials for Tissue Engineering, Advanced Healthcare Materials, 2018, 7(7), 1701095.

[12] Placone JK, Engler AJ, Recent Advances in Extrusion-Based 3D Printing for Biomedical Applications, Advanced Healthcare Materials, 2018, 7(8), 1701161.

[13] Ma HS, Feng C, Chang J, Wu CT, 3D-printed bioceramic scaffolds: From bone tissue engineering to tumor therapy, Acta Biomaterialia, 2018, 79, 37-59.

[14] 3D printing of ceramic-based scaffolds for bone tissue engineering: an overview. Du XY, Fu SY, Zhu YF, Journal of Materials Chemistry B, 2018, 6(27), 4397-4412.

[15] Liu C, Zeng Y, Kankala RK, Zhang S, Chen A, Wang SB. Characterization and Preliminary Biological Evaluation of 3D-Printed Porous Scaffolds for Engineering Bone Tissues, Materials, 2018, 11(10): 1832.

[16] Chen L, Deng CJ, Li JY, Yao QQ, Chang J, Wang LM, Wu CT. 3D printing of a lithium-calcium-silicate crystal bioscaffold with dual bioactivities for osteochondral interface reconstruction, Biomaterials, 2019, 196: SI 138-150.

[17] Fina F, Goyanes A, Gaisford S, Basit AW. Selective laser sintering (SLS) 3D printing of medicines. International Journal of Pharmaceutics, 2017, 529(1-2): 285-293.

[18] Luo Y, Li Y, Qin X, Wa Q, 3D printing of concentrated alginate/gelatin scaffolds with homogeneous nano apatite coating for bone tissue engineering, Materials & Design, 2018, 146: 12-19.

[19] Li H, Tan C, Li L, Review of 3D printable hydrogels and constructs， Materials & Design, 2018, 159: 20-38.

[20] Lee H, Yang GH, Kim M, Lee JY, Huh JT, Kim GH, Fabrication of micro/nanoporous collagen/dECM/silk-fibroin biocomposite scaffolds using a low temperature 3D printing process for bone tissue regeneration, Materials Science and Engineering: C, 2018, 84: 140-147.

[21] Adamkiewicz M, Rubinsky B, Cryogenic 3D printing for tissue engineeringCryobiology, 2015, 71(3): 518-521.

[22] Zhang Y, Wang C, Fu L, Ye S, Wang M, Zhou Y, Fabrication and Application of Novel Porous Scaffold in Situ-Loaded Graphene Oxide and Osteogenic Peptide by Cryogenic 3D Printing for Repairing Critical-Sized Bone Defect, 2019, Molecules, 24: 1669.

[23] Lai Y, Cao H, Wang X, Chen S, Zhang M, Wang N, Yao Z, Dai Y, Xie X, Zhang P, Yao X, Qin L, Porous composite scaffold incorporating osteogenic phytomolecule icariin for promoting skeletal regeneration in challenging osteonecrotic bone in rabbits, Biomaterials, 2018, 153: 1-13.

[24] Shim JH, Jang KM, Hahn SK, Park JY, Jung H, Oh K, Park KM, Yeom J, Park SH, Kim SW, Wang JH, Kim K, Cho DW, Three-dimensional bioprinting of multilayered constructs containing human mesenchymal stromal cells for osteochondral tissue regeneration in the rabbit knee joint, Biofabrication, 2016, 8(1), 014102.

[25] Correa D, Lietman SA, Articular cartilage repair: Current needs, methods and research directions, Seminars in Cell & Developmental Biology, 2017, 62, 67-77.

[26] Lee N, Robinson J, Lu H, Biomimetic strategies for engineering composite tissues, Current Opinion in Biotechnology, 2016, 40, 64-74.

[27] Rezwan K, Chen QZ, Blaker JJ, Boccaccini AR, Biodegradable and bioactive porous polymer/inorganic composite scaffolds for bone tissue engineering, Biomaterials,2006, 27(18): 3413-3431.

[28] Beck EC, Barragan M, Tadros MH, Gehrke SH, Detamore MS. Approaching the compressive modulus of articular cartilage with a decellularized cartilage-based hydrogel, Acta Biomaterialia, 2016, 38: 94-105.

[29] Yao H, Kang JP, Li WC , Liu J, Xie RJ, Wang YJ, Liu S, Wang DA, Ren L, Novel beta-TCP/PVA bilayered hydrogels with considerable physical and bio-functional properties for osteochondral repair, Biomedical Materials, 2018, 13(1), 015012.

[30] Wada S, Kitamura N, Nonoyama T, Kiyama R, Kurokawa T, Gong JP, Yasuda K, Hydroxyapatite-coated double network hydrogel directly bondable to the bone: Biological and biomechanical evaluations of the bonding property in an osteochondral defect, Acta

Biomaterialia, 2016,44, 125-134.

[31] Harley BA, Lynn AK, Wissner-Gross Z, Bonfield W, Yannas IV, Gibson LJ, Design of a multiphase osteochondral scaffold. II. Fabrication of a mineralized collagen-glycosaminoglycan scaffold, Journal of Biomedical Materials Research Part A, 2010, 92A(3), 1066-1077.

[32] Jia SJ, Wang J, Zhang T, Pan WM, Li Z, He X, Yang CF, Wu QN, Sun W, Xiong Z, Hao DJ, Multilayered Scaffold with a Compact Interfacial Layer Enhances Osteochondral Defect Repair, ACS Applied Materials & Interfaces, 2018, 10(24), 20296-20305.

[33] Shen S, Chen MX, Guo WM, Li HJ, Li X, Huang SQ, Luo XJ, Wang ZY, Wen Y, Yuan ZG, Zhang B, Peng LQ, Gao C, Guo QY, Liu SY, Zhuo NQ, Three Dimensional Printing-Based Strategies for Functional Cartilage Regeneration, Tissue Engineering Part B-Rreviews, 2019 5(3), 187-201.

[34] Di Luca A, Klein-Gunnewiek M, Vancso JG, van Blitterswijk CA, Benetti EM, Moroni L, Covalent Binding of Bone Morphogenetic Protein-2 and Transforming Growth Factor-3 to 3D Plotted Scaffolds for Osteochondral Tissue Regeneration, Biotechnology Journal, 2017, 12(12), SI1700072.

[35] Studle C, Vallmajo-Martin Q, Haumer A, Guerrero J, Centola M, Mehrkens A, Schaefer DJ, Ehrbar M, Barbero A, Martin I, Spatially confined induction of endochondral ossification by functionalized hydrogels for ectopic engineering of osteochondral tissues, Biomaterials, 2018, 171, 219-229.

[36] Wang C, Zhao QL, Wang M, Cryogenic 3D printing for producing hierarchical porous and rhBMP-2loaded Ca-P/PLLA nanocomposite scaffolds for bone tissue engineering2017, 9(2), 025031.

[37] Wang W, Passarini JR, Nalesso PRL, Musson D, Cornish J, Mendonca F, Caetano GF,

Bartolo P, Engineered 3D printed poly(epsilon-caprolactone)/graphene scaffolds for bone tissue engineering,Materials Science & Engineering C-Materials for Biological Applications, 2019, 100, 759-770.

[38] Zhao QL, Wang J, Cui HQ, Chen HX, Wang YL, Du XM, Programmed Shape-Morphing Scaffolds Enabling Facile 3D Endothelialization. Advanced Functional Materials, 2018, 28(29), 1801027.

[39] Bao M, Wang XL, Yuan HH, Lou XX, Zhao QH, Zhang YZ, HAp incorporated ultrafine polymeric fibers with shape memory effect for potential use in bone screw hole healing. Journal of Materials Chemistry B, 2016, 4(31), 5308-5320.

[40] Zhou X, Esworthy T, Lee S, Miao S, Cui H, Plesiniak M, Fenniri H, Webster T, Rao RD, Zhang LG, 3D Printed scaffolds with hierarchical biomimetic structure for osteochondral regeneration,Nanomedicine: Nanotechnology, Biology and Medicine,2019, 19: 58-70.

[41] Deng C, Chang J, Wu C, Bioactive scaffolds for osteochondral regenerationJournal of Orthopaedic Translation, 2019, 17: 15-25.

[42] Bunpetch V, Zhang X, Li T, Lin J, Maswikiti EP, Wu Y, Cai D, Li J, Zhang S, Wu C, Ouyang H, Silicate-based bioceramic scaffolds for dual-lineage regeneration of osteochondral defect,Biomaterials, 2019, 192: 323-333.

[43] Dong Y, Sun X, Zhang Z, Liu Y, Zhang L, Zhang X, Huang Y, Zhao Y, Qi C, Midgley AC, WangS, Yang Q, Regional and sustained dual-release of growth factors from biomimetic tri-layered scaffolds for the repair of large-scale osteochondral defects, Applied Materials Today,2020, 19: 100548.